Uniaxial drawing of poly(vinyl alcohol)/graphene oxide nanocomposites

Morimune, Seira
Kotera, Masaru
Nishino, Takashi
Goto, Takuya

(Citation)
Carbon,70:38-45

(Issue Date)
2014-04

(Resource Type)
journal article

(Version)
Accepted Manuscript

(URL)
https://hdl.handle.net/20.500.14094/90004810

Uniaxial Drawing of Poly (vinyl alcohol)/Graphene Oxide Nanocomposites

Seira Morimune†, Masaru Kotera†, Takashi Nishino† and Takuya Goto‡*

† Department of Chemical Science and Engineering, Graduate School of Engineering, Kobe University, Rokko, Nada, Kobe 657-8501 (Japan)

‡ Mitsubishi Gas Chem. Inc., Niijuku, Katsushika, Tokyo 125-8601 (Japan)

*Corresponding Author. Tel: +81-78-803-6164. E-mail: tnishino@kobe-u.ac.jp (Takashi Nishino)

ABSTRACT.

The unique potential of graphene oxide (GO) was exploited in the nanocomposites by a simple uniaxial drawing (up to 3 times) of poly (vinyl alcohol) (PVA)/GO nanocomposites with a small amount loading of GO. From X-ray diffraction images, the PVA crystallites were found to be oriented parallel to the drawn direction. At the same time, exfoliated GO platelets were found to be aligned parallel to the film surface. Compared with the properties of the as-cast nanocomposites, those of the uniaxially drawn nanocomposites were found to be remarkably enhanced. For the mechanical properties, not only the Young´s modulus and tensile strength, but also the toughness of the nanocomposites increased by the uniaxial drawing. It was revealed that 260 % increase of the toughness was achieved for the drawn nanocomposite with 1 % w/w GO loading. Significant suppression of the swelling in water brought the excellent barrier properties against water, which exceeded that of the conventional high-barrier polymer, such as poly (vinylidene chloride). We revealed that this simple, fast and environmentally friendly process of uniaxial drawing exploit the excellent properties and high aspect ratio of GO in the nanocomposites.

TEXT.

1. Introduction

Among the composites materials, polymer nanocomposites have attracted a great deal of attention due to their high performances. The remarkable enhancements in various properties by the incorporation of a small amount of nanofillers have often been reported, therefore, they have been expected as alternatives for pure polymers or conventional micro-filler composites. Since Toyota Central R&D Labs., Inc. first reported the development of the nanocomposites composed of nylon 6 and clay,[1–4] many kinds of nanofillers were incorporated in polymer matrices.[5–9] In recent years, one of the most highly attractive nanofillers is graphene.[10,11] Graphene is a single atom thick layer of carbon which shows extremely high performances in its properties, such as mechanical, thermal and electronic properties.[12–15] In order to produce good interactions between graphene and polymer matrices, chemical modification of graphene has been widely conducted and rich varieties of graphene derivatives have been developed.[11] Chemically modified graphene derivatives are often processed from graphene oxide (GO), which is prepared during the chemical preparation of graphene through the oxidation of graphite.[16] GO possesses oxygen-containing functional groups on the base plane of graphene, thus GO shows hydrophilic affinity.[17,18] Therefore, aqueous process for the preparation of nanocomposites can readily achieve the nano-dispersion of GO.[19]

In our previous study, we selected poly (vinyl alcohol) (PVA), well known as a water soluble polymer, as a matrix and prepared PVA/GO nanocomposites using a simple casting method through the aqueous medium.[20] We revealed that the GO platelets were highly exfoliated and nano-dispersed in the polymer matrix, and the as-cast PVA/GO nanocomposites showed the excellent properties. So far, several researches on PVA/GO nanocomposites have been reported which provided several methods of using water as a processing medium.[21–24] Zhao *et. al.* prepared the nanocomposites with high content of GO

using layer-by-layer assembly and showed the remarkable increases in elastic modulus and hardness.[24] The high content PVA/GO nanocomposite was also prepared by vacuum-assisted self-assembly.[25] Both of these techniques brought the layered nanocomposites.[26,27] The strong interaction between polymer and filler were produced by these processes with the high in-plane alignment of GO, which results in the extremely high stiffness of the composites. Polymer nanocomposites reinforced by highly aligned layered nanofillers with high content were often investigated as artificial models of nacre, which is the composition of highly aligned inorganic aragonite platelets and protein. It was reported that the high stiffness comparable to that of nacre was achieved by layer-by-layer process of PVA/clay nanocomposites.[26] However, it is difficult to control the amount of the fillers by these methods, and the filler content has no choice but to be high, and intrinsically these are time/cost consuming process.

Generally, the alignment of the filler with high aspect ratio has a critical effect on the properties of composites.[28,29] For example, the alignment of the layered particles in the direction parallel to the film surface can produce the significant barrier properties.[30] In this study, orientation control of the PVA/GO nanocomposites was done by the uniaxial drawing of the as-cast nanocomposites. The casting method enables to control the GO content to be 0–1 % w/w. GO is expected to align parallel to the film surface by the simple uniaxial drawing. The effects of the uniaxial drawing on the structure and properties of the nanocomposites were investigated. This is an attempt to maximize the excellent properties of GO with a minimum content of GO.

2. Experimental

2.1 Materials

GO aqueous suspension (1 % w/w) was supplied from Mitsubishi Gas Chemical, Inc. (Tokyo, Japan). GO in the aqueous medium was synthesized from graphite using the method based on Hummers' method.[31] PVA powder ("Gohsenol NH-18", Nippon Synthetic Chemical Industry Co., Ltd., Osaka, Japan) was used with a degree of polymerization of 1,800 and a degree of saponification greater than 99 %.

2.2 Sample preparation

The PVA/GO nanocomposites were prepared by solvent casting method. The details of the nanocomposite preparation are described in our previous report.[20] The as-cast nanocomposites were put into an oven at 160 ºC for 15 min, subsequently, uniaxially drawn. The draw ratio was fixed at 3 times and the thickness of the drawn films was 60 μm.

2.3 Characterization

X-ray generator (RINT2100, Rigaku, Tokyo, Japan) was operated at 40 kV and 20 mA. X-ray diffraction profiles were obtained by irradiating the samples by Ni-filtered CuKα radiation. The scanning speed was 1.0 degree/min, and the $2\theta/\theta$ scan data were collected at 0.02 degree intervals. X-ray diffraction images were taken with a flat camera.

The cross section of the uniaxially drawn PVA/GO nanocomposite wiht 1 % w/w GO loading was observed using a field emission scanning electron microscope (FE-SEM) (JEOL, JSM-7500F) at an accelerating voltage of 2 kV and emission current of 10 μA. Osmium tetroxide was deposited on the sample surface prior to observation.

Tensile test of the drawn PVA/GO nanocomposites were performed using Autograph AGS-1kND (Shimadzu Co., Kyoto, Japan). The cross head speed was 2 mm/min and the initial length was 20 mm.

More than 10 specimens were tested for each sample. The toughness (K) was calculated using the following equation:

$$K = \int_{\varepsilon=0}^{\varepsilon=\varepsilon_{max}} \sigma \cdot d\varepsilon / \rho \qquad \text{(J/g)} \tag{1}$$

where, σ is stress (Pa=J/m^3), ε is strain (-). and ρ is density (g/m^3).

The dynamic mechanical analyses were performed using a dynamic mechanical analyzer, DVA-220S (ITK Co., Ltd., Osaka, Japan). A heating rate of 6 °C/min with a frequency of 10 Hz was employed under nitrogen flow.

Differential scanning calorimetry (DSC) was carried out using a differential scanning calorimeter (DSC-220CU, Seiko Instruments Inc., Chiba, Japan). The melting points (T_m) of the nanocomposites were determined as the endotherm peak temperature. The thermal decomposition temperature (T_d) was measured with a thermogravimeter (TG/DTA-220CU, Seiko Instruments Inc., Chiba, Japan). The T_d was defined as the temperature at which the substance had a 5 wt% thermal weight loss. DSC and TG were performed under nitrogen flow with a heating rate of 10 °C/min. Thermal diffusivity (α) was obtained by Thermowave Analyzer TA3 (Bethel Co., Ltd., Ibaraki, Japan) under periodic laser heating. The α of in-plane direction was measured at room temperature.

The swelling ratio was determined by immersing the specimens in distilled water at 30 ºC and was defined as the weight gain of the specimens as follows:

$$\text{Swelling ratio} = W/W_0 \tag{2}$$

where, W_0 and W is the weight of the specimen before and after swelling, respectively. Then the diffusion coefficient of water (D) was determined using the following equation:[32,33]

$$D = \pi\left(\frac{Qr}{4}\right)^2 \quad \text{(m}^2\text{/s)} \tag{3}$$

where Q is the initial slope of the linear approximation obtained by plotting the swelling ratio versus the square root of the swelling time and r is the thickness of the specimens.

3. Results and Discussion

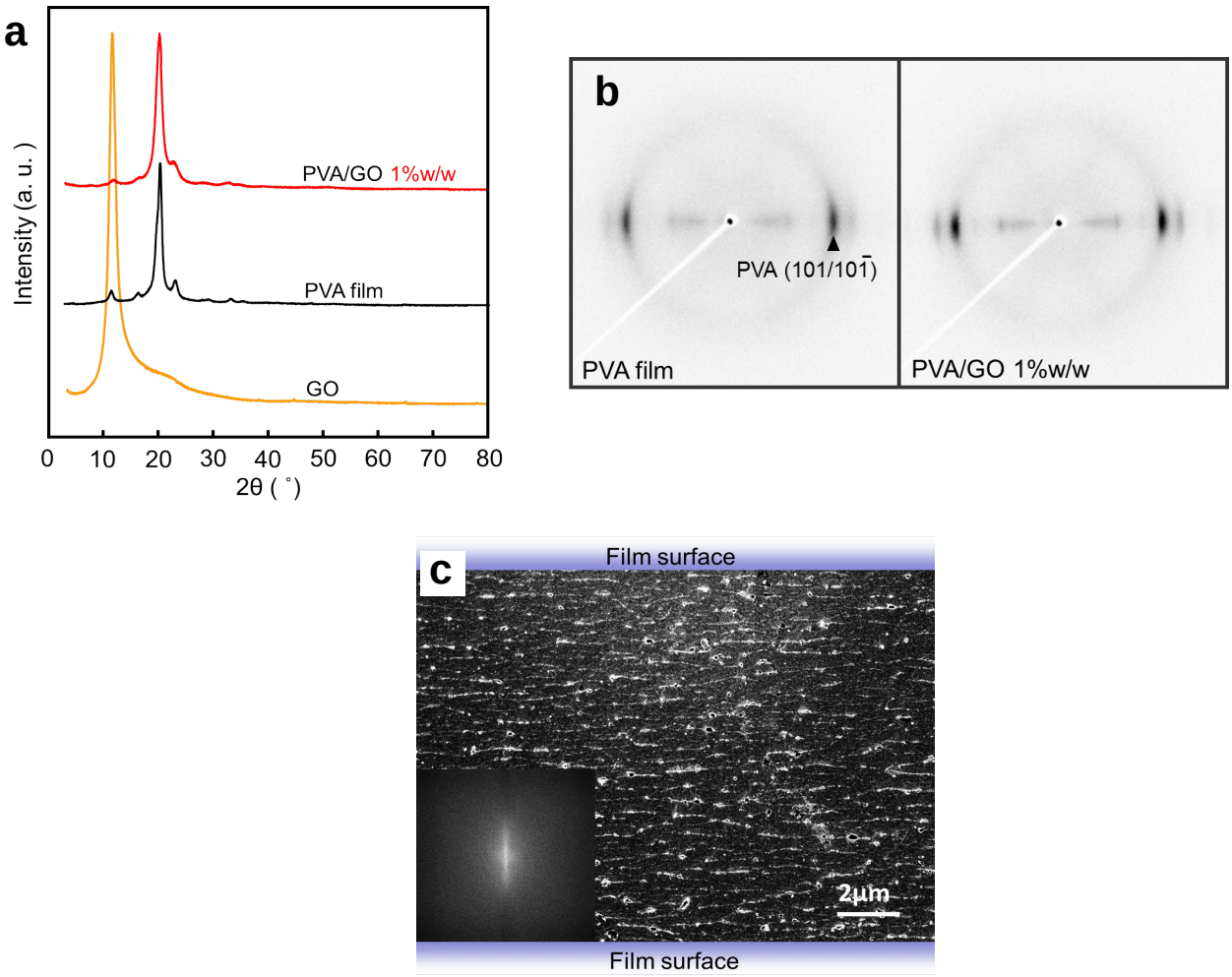

Figure 1. (a) Equatorial X-ray diffraction profiles of the uniaxially drawn PVA film, PVA/GO nanocomposites and annealed GO (160 ºC, 15 min); **(b)** X-ray diffraction images of the uniaxially drawn PVA film and PVA/GO nanocomposite with 1 % w/w GO loading; **(c)** FE-SEM image of cross section of uniaxially drawn PVA/GO nanocomposite with 1 % w/w loading. The result of 2D Fast Fourier Transform was superimposed in the lower left corner.

3.1 Characterization

Figure 1a shows the equatorial X-ray diffraction profiles of the uniaxially drawn PVA film, PVA/GO nanocomposite (1 % w/w) and annealed GO. The annealed GO was prepared by drying the aqueous suspension and dried in an oven at the same condition of drawing (160 ºC, 15 min). Due to the

increasing of the crystallinity of PVA by annealing, both PVA film and the nanocomposites showed sharp peaks. On the profile of GO, the characteristic peak of 001 reflection appeared clearly at 2θ =10.1 º corresponding to the interlayer distance of 8.8 Å, which is larger than that of graphite oxide (6.7 Å).[34] Compared to the interlayer distance of natural graphite (3.35 Å), that of graphite oxide and of GO were relatively large. This shows the presence of the oxygen containing functional groups which were located between the interlayers of graphite oxide and of GO.[35] In addition, the appearance of the 001 reflection indicates that GO formed graphite (graphite oxide) like structure during the drying process, mainly by van der Waals force, while it was exfoliated in the aqueous suspension.

X-ray diffraction images were taken in order to assess the orientation in the uniaxially drawn PVA film and PVA/GO nanocomposites (Figure 1b). The peak assigned to 101/10$\bar{1}$ reflection of PVA appeared clearly for both the PVA film and the nanocomposites. The uniaxially drawn samples showed equatorial arc patterns, indicating that the PVA crystallites were oriented parallel to the drawn direction. The alignment of GO was observed as bright lines in the FE-SEM image as shown in Figure 1c. The result of 2D Fast Fourier Transform was superimposed in the lower left corner. Previously, we showed that GO platelets were partially aligned parallel to the film surface in the as-cast nanocomposites.[20] In the case of the uniaxially drawn nanocomposites, GO platelets were found to be almost fully aligned parallel to the film surface in the overall structure. It is well known that the orientation of the polymer crystallites and the alignment of the filler, especially the filler with high aspect ratio, being the large effect on the properties of the nanocomposites. [36,37]

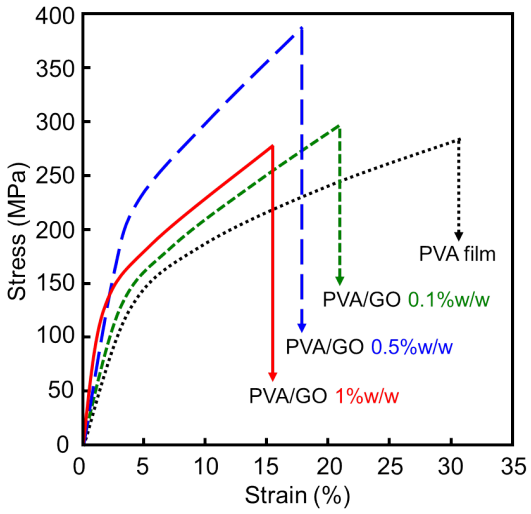

Figure 2. Stress (σ) - strain (ε) curves of the uniaxially drawn PVA film and PVA/GO nanocomposites.

3.2 Mechanical properties

Figure 2 shows the stress (σ) – strain (ε) curves of the uniaxially drawn PVA film and PVA/GO nanocomposites. The Young's modulus (E) of the drawn nanocomposite increased with increasing of GO content, and it was found to be 160 % higher than that of drawn PVA film with only 1 % w/w GO loading (Supplementary Table 1). For the tensile strength (σ_{max}), the nanocomposite with GO 0.5 % w/w showed the highest value of 392 MPa, which was 37 % higher than that of drawn PVA film (Supplementary Table 1). On the other hand, for the elongation at break (ε_{max}), the drawn nanocomposites moderately decreased with increasing of the GO content.

Figure 3a-d show the E, σ_{max}, ε_{max} and K values of the drawn nanocomposites and the as-cast nanocomposites[20] as a function of GO content. It was obvious that the E and σ_{max} values remarkably increased by the drawing (Figure 3ab). The E and σ_{max} values of the drawn PVA film were found to be 89 % and 202 % higher than those of the as-cast PVA film, respectively. These correspond that the PVA crystallites in the drawn film were highly oriented as shown above. In the drawn nanocomposites, the effective stress transfer was achieved by the highly oriented PVA crystallites and highly aligned GO.

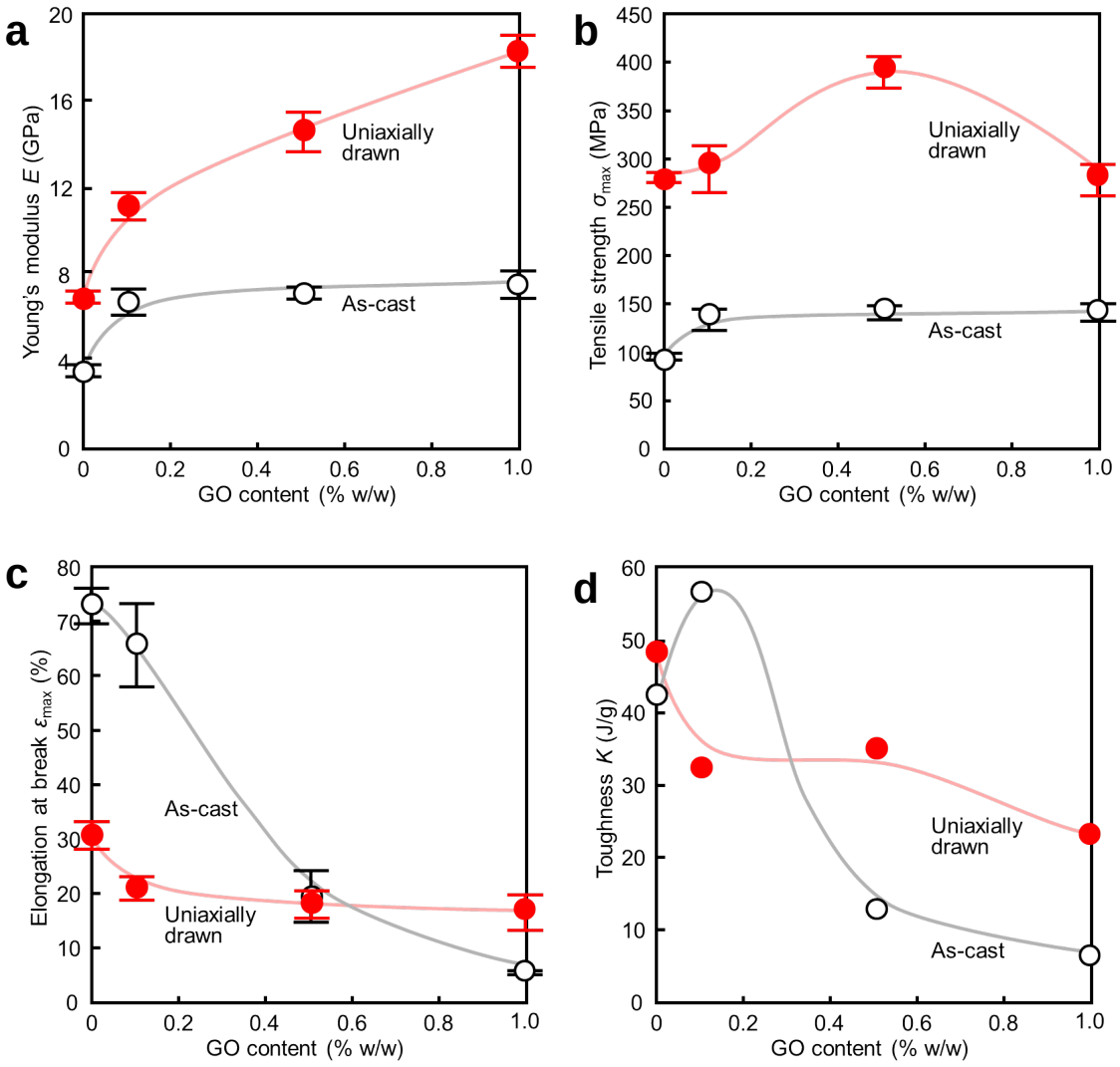

Figure 3. (a) Young's modulus (E), **(b)** tensile strength (σ_{max}), **(c)** elongation at break (ε_{max}) and **(d)** toughness (K) of the uniaxially drawn PVA/GO nanocomposites and the as-cast PVA/GO nanocomposites as a function of GO content.

Therefore, the nanocomposites were revealed to show remarkable increase in the E and σ_{max} values by the drawing.

As previously mentioned, the ε_{max} value of the as-cast composite decreased abruptly with the GO loading, however, that of the drawn nanocomposite was hold even after the incorporation of GO. Finally, the ε_{max} value of the drawn nanocomposite with 1 % w/w GO loading was found to be higher than that

of the as-cast nanocomposite (Figure 3c). Therefore, as shown in Figure 3d, it was revealed that the toughness (*K*) of the drawn nanocomposites tended to maintain higher value. For example, compared to the as-cast nanocomposites, the *K* value of the nanocomposites increased 170% and 260 % with 0.5 % w/w and 1 % w/w GO loading, respectively. Generally, the interface between filler and matrix often causes the initial crack due to the high stress concentration at the filler edges. The as-cast PVA/GO nanocomposites showed large decrease in ε_{max} value which was caused by the random alignment of GO with its anisotropic morphology.[20,38] On the other hand, for the drawn PVA/GO nanocomposites, the stress concentration at the interface was decreased by the parallel alignment of GO and the crack propagation in the direction perpendicular to the film surface was also prevented by the aligned GO platelets. Wang *et. al*.[39] showed the fracture mechanism in the epoxy/clay nanocomposite. They revealed that the clay layers, which aligned perpendicular to the direction of the crack propagation, hindered the crack propagation. Therefore, it was assumed that the aligned GO was also acted as a barrier against the crack propagation.

Figure 4 shows the temperature dependence of the storage modulus (*E´*) and the mechanical tanδ of the uniaxially drawn PVA film and PVA/GO nanocomposites. The dispersion at above 100 ºC, the main dispersion at 73 – 82 ºC and the lower temperature dispersion (approximately 0 ˚C) in the mechanical tanδ is so-called α_c dispersion, α_a dispersion and β dispersion, respectively. The intensity of both α_a and β dispersions were found to be suppressed by the addition of GO. These suggest that the mobility of PVA molecular chains in amorphous region was largely restricted by the aligned GO platelets, which functioned as the excellent reinforcement with their rigid structure. In addition, the peek temperature of the α_c dispersion, which was attributed to the PVA crystal relaxation, was found to be increased by the incorporation of GO. Previously, we reported that GO largely affects the amorphous region than the

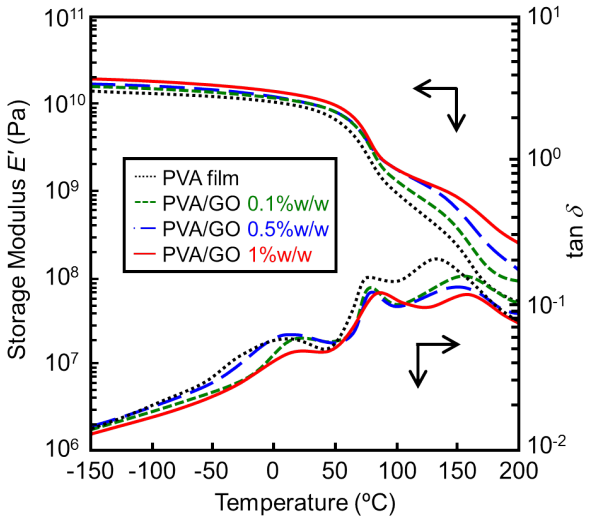

Figure 4. Temperature dependence of storage modulus (*E´*) and mechanical tan*δ* of the uniaxially drawn PVA film and PVA/GO nanocomposites.

crystalline regions of the PVA matrix for the as-cast nanocomposites. [20] On the other hand, in the drawn nanocomposites, the reinforcement effect of GO was revealed to be effective not only for the amorphous region but also for the crystalline regions.

From the results of the *E´*, it is clear that the nanocomposites maintained the high *E´* within the whole temperature range (-150 – 200 ˚C), and the decrease of *E´* value with temperature over the glass transition (T_g) was effectively suppressed. This result also supported that the highly aligned GO platelets largely suppressed the mobility of PVA molecular chains for the drawn nanocomposites.

In addition, the α_a dispersion in the mechanical tan*δ*, corresponding to the T_g of the PVA matrix, as well as the α_c dispersion, shifted to higher temperature for the nanocomposites with the increasing of the GO content.[40] The T_g of the uniaxially drawn nanocomposites with 1 % w/w was found to be 9 ºC higher than that of uniaxially drawn PVA film, and 20 ºC higher than that of as-cast PVA film (Supplementary Table 2).

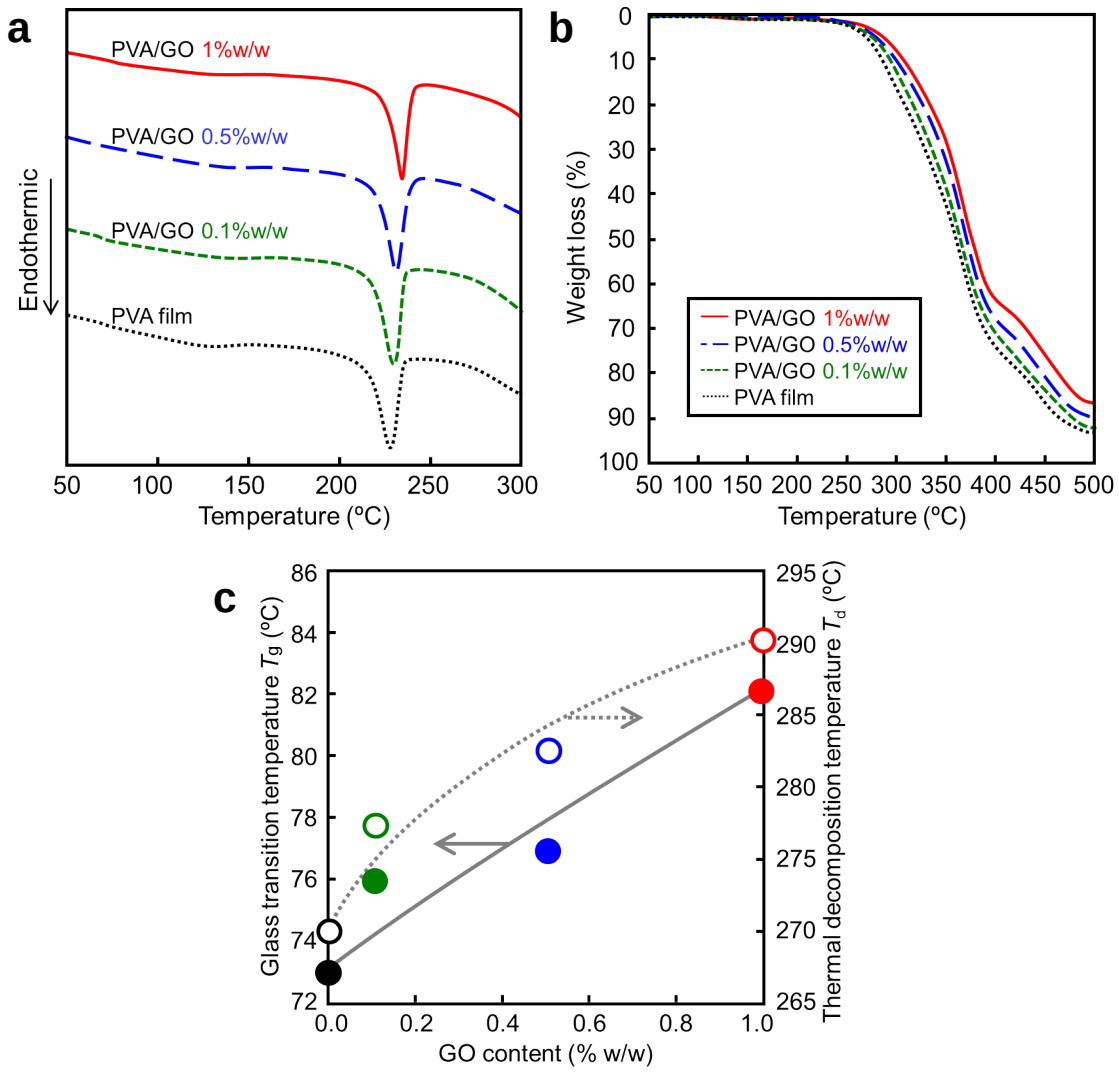

Figure 5. (a) DSC thermograms of the uniaxially drawn PVA film and PVA/GO nanocomposites; **(b)** Thermogravimetric traces of the uniaxially drawn PVA film and PVA/GO nanocomposites; **(c)** Glass transition temperature (T_g) and thermal decomposition temperature (T_d) of the uniaxially drawn PVA film and PVA/GO nanocomposites.

3.3 Thermal properties

Figure 5a shows the DSC thermograms of the uniaxially drawn PVA film and PVA/GO nanocomposites. The endotherm at 227 – 232 °C assigned as the melting temperature (T_m) of PVA. Due to the increase in the crystallinity of PVA, the drawn nanocomposites showed sharper endotherms than

that of the PVA film. On the other hand, there was no obvious change in T_m by the incorporation of GO for uniaxially drawn nanocomposites. This result suggests that GO had little effect on the PVA crystallites size while the crystallinity was increased and the molecular motion of PVA was suppressed by the incorporation of GO.

The results in thermogravimetry showed a large difference between the PVA film and the nanocomposites. The thermogravimetric traces of the uniaxially drawn PVA film and PVA/GO nanocomposites are shown in Figure 5b. As well as T_g, it was revealed that the T_d remarkably increased for the drawn nanocomposite (Figure 5c). The T_d of the drawn nanocomposite with 1 % w/w GO loading showed 20 ºC higher value than that of the drawn PVA film. Furthermore, it was 27 ºC higher than that of the as-cast PVA film (Supporting Table 2).[20] This excellent thermal resistance was achieved by nano dispersed and highly aligned GO with its high aspect ratio, which interrupted the volatile decomposition products passing through the material.[26]

Table 1. In-plane thermal diffusivity (α) of the uniaxially drawn PVA film, PVA/GO nanocomposites and the as-cast PVA film.[20]

	α (//*)	α (⊥**)
	$\times 10^{-6}$ m^2/s	$\times 10^{-6}$ m^2/s
Uniaxially drawn PVA film	0.879	0.449
Uniaxially drawn PVA/GO 1%w/w	1.089	0.550
As-cast PVA film[20]	0.405	0.405

*//: Parallel to the drawn direction. **⊥: Perpendicular to the drawn direction.

The in-plane thermal diffusivity (α) of the drawn nanocomposites was shown in Table 1. The in-plane α value parallel and perpendicular to the drawn direction were evaluated. In the parallel direction, the α value of the PVA film was largely increased by the uniaxial drawing, while there was little difference in the perpendicular direction. In addition, for the uniaxially drawn samples, the further increase was observed for the nanocomposites. Pietralla *et. al*. showed that the α value of uniaxially stretched low density polyethylene (PE) increased with the draw ratio.[41,42] They mentioned that, in thed polymer, the thermal diffusion in the drawn direction was dominated by the oriented polymer crystallites in the crystalline regions. It was suggested that, in the uniaxially drawn nanocomposites, in addition to the efficient heat transfer brought by the highly oriented PVA crystallites, the highly aligned GO also promoted the heat transfer and achieve the significant increase in the thermal conductivity.

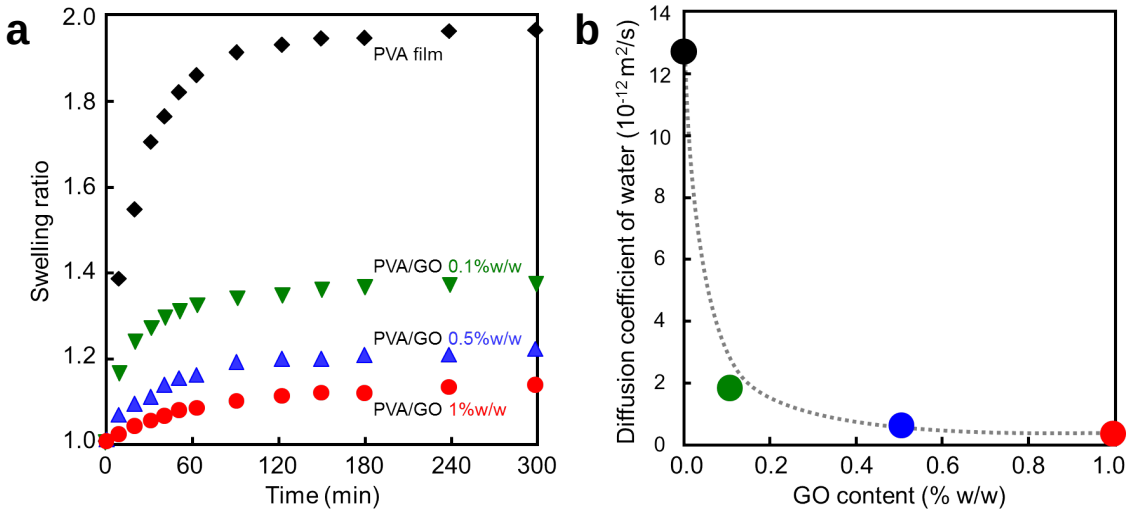

Figure 6. (a) Swelling ratio of the uniaxially drawn PVA film and PVA/GO nanocomposites in water at 30 ˚C; **(b)** Water diffusion coefficient of the uniaxially drawn PVA film and PVA/GO nanocomposites.

3.4 Barrier properties

Figure 6a shows the swelling ratio of the uniaxially drawn PVA film and PVA/GO nanocomposites in distilled water at 30 ºC. It was revealed that the swelling ratio was largely suppressed by the incorporation of GO. For example, compared with the drawn PVA film, the plateau swelling ratio was suppressed by 42 % for the drawn nanocomposite with 1 % w/w GO loading. This indicates that, corresponding to the DMA results, the aligned GO platelets effectively suppressed the molecular motion of PVA and prevented the swelling of the whole material.

Next, the diffusion coefficient of water was calculated from the initial gradient of the swelling ratio curve (Figure 6b). As well as the swelling ratio, the drawn nanocomposites showed the significant reduction in the diffusion coefficient of water. The addition of GO 0.1 % w/w suppressed the diffusion coefficient by 85 % compared with that of the drawn PVA film. Furthermore, the diffusion coefficient of the drawn nanocomposite with 1 % w/w GO loading was found to be almost two orders of magnitude lower than that of the drawn PVA film. In our previous study, the as cast nanocomposites with 1 % w/w

GO loading was revealed to show the diffusion coefficient comparable to poly (vinylidene chloride) (PVDC), which is well known for its high barrier properties and is often used as a raw material for plastic wrap.[20,43] In this study, regarding the nanocomposites reinforced by 1 % w/w GO loading, the diffusion coefficient was suppressed by 99 % by the drawing. In other words, the drawn nanocomposites achieved to suppress the diffusion coefficient to much lower value than that of PVDC with only 1 % w/w GO loading. This superior barrier property was brought by the synergetic effect of PVA and GO in the drawn nanocomposite. The nanodispersed and highly aligned GO platelets, together with the highly crystallized and highly oriented PVA, significantly prevented the penetration of water into the nanocomposites.

4. Conclusions

By the uniaxial drawing of the PVA/GO nanocomposites, the PVA crystallites oriented parallel to the drawn direction. At the same time, the GO platelets highly aligned parallel to the film surface. For the mechanical properties, the uniaxially drawn PVA/GO nanocomposites were found to show high E and σ_{max} value. In addition, the K value of the uniaxially drawn nanocomposites remarkably increased compared with those of as-cast nanocomposites. Furthermore, it was revealed that the drawn nanocomposites possess excellent thermal resistance and water resistance.

The high aspect ratio of GO and its rigid structure was effectively applied to the nanocomposites by uniaxial drawing, resulting in the surprising enhancement in their properties. We revealed that the optimization of PVA/GO nanocomposites was achieved by this simple, fast and environmentally friendly process.

Figure captions

Figure 1. (a) Equatorial X-ray diffraction profiles of the uniaxially drawn PVA film, PVA/GO nanocomposites and annealed GO (160 ºC, 15 min); **(b)** X-ray diffraction images of the uniaxially drawn PVA film and PVA/GO nanocomposite with 1 % w/w GO loading; **(c)** FE-SEM image of cross section of uniaxially drawn PVA/GO nanocomposite with 1 % w/w loading. The result of 2D Fast Fourier Transform was superimposed in the lower left corner.

Figure 2. Stress (σ) - strain (ε) curves of the uniaxially drawn PVA film and PVA/GO nanocomposites.

Figure 3. (a) Young's modulus (E), **(b)** tensile strength (σ_{max}), **(c)** elongation at break (ε_{max}) and **(d)** toughness (K) of the uniaxially drawn PVA/GO nanocomposites and the as-cast PVA/GO nanocomposites as a function of GO content.

Figure 4. Temperature dependence of storage modulus (E') and mechanical tanδ of the uniaxially drawn PVA film and PVA/GO nanocomposites.

Figure 5. (a) DSC thermograms of the uniaxially drawn PVA film and PVA/GO nanocomposites; **(b)** Thermogravimetric traces of the uniaxially drawn PVA film and PVA/GO nanocomposites; **(c)** Glass transition temperature (T_g) and thermal decomposition temperature (T_d) of the uniaxially drawn PVA film and PVA/GO nanocomposites.

Figure 6. (a) Swelling ratio of the uniaxially drawn PVA film and PVA/GO nanocomposites in water at 30 ˚C; (**b)** Water diffusion coefficient of the uniaxially drawn PVA film and PVA/GO nanocomposites.

Table 1. In-plane thermal diffusivity (α) of the uniaxially drawn PVA film, PVA/GO nanocomposites and the as-cast PVA film.[20]

Acknowledgment

This work was supported by Grant-in-Aid for Scientific Research (A) from the Ministry of Education, Culture, Sports, Science and Technology (MEXT) of Japan and Grant-in-Aid for Japan Society for the Promotion of Science (JSPS) Fellows.

REFERENCES

[1] Usuki, A.; Kojima, Y.; Kawasumi, M.; Okada, A.; Fukushima, Y.; Kurauchi, T. et al. Synthesis of Nylon6 Clay Hybrid. *J. Mater. Res.*, 1993, 8 (5), 1179–1184.

[2] Kojima, Y.; Usuki, A.; Kawasumi, M.; Okada, A.; Fukushima, Y.; Kurauchi, T.; et al. Mechanical Properties of Nylon6-Clay Hybrid. *J. Mater. Res.*, 1993, 8 (5), 1185–1189.

[3] Kojima, Y.; Usuki, A.; Kawasumi, M.; Okada, A.; Fukushima, Y.; Kurauchi, T. et al. Synthesis of Nylon6-Clay Hybrid by Montmorillonite Intercalated with ε-Caprolactam. *J. Polym. Sci. Part A: Polym. Chem.*, 1993, 31 (4), 983–986.

[4] Kojima, Y.; Usuki, A.; Kawasumi, M.; Okada, A.; Fukushima, Y.; Kurauchi, T. et al. One-Pot Synthesis of Nylon6-Clay Hybrid. *J. Polym. Sci. Part A: Polym. Chem.*, 1993, 31 (7), 1775–1778.

[5] Okada, A.; Usuki, A. Twenty Years of Polymer-Clay Nanocomposites. *Macromol. Mater. Eng.*, 2006, 291 (12), 1449–1476.

[6] Moniruzzaman, M.; Winey, K. I. Polymer Nanocomposites Containing Carbon Nanotubes. *Macromolecules*, 2006, 39 (16), 5194–5205.

[7] Paul, D. R.; Robeson, L. M. Polymer Nanotechnology: Nanocomposites. *Polymer*, 2008, 49 (15), 3187–3204.

[8] Morimune, S.; Kotera, M.; Nishino, T. Stress Transfer of Poly (vinyl alcohol) Montmorillonite Nanocomposite using X-ray Diffraction. *J. Adh. Soc. Jpn.*, 2010, 46 (9), 320–325.

[9] Morimune, S.; Kotera, M.; Nishino, T.; Goto, K.; Hata, K. Poly (vinyl alcohol) Nanocomposites with Nanodiamond. *Macromolecules*, 2011, 44 (11), 4415–4421.

[10] Kim, H.; Abdala, A. A.; Macosko, W. C. Graphene/Polymer Nanocomposites. *Macromolecules*, 2010, 43 (16), 6515–6530.

[11] Stankovich, S.; Dikin, D. A.; Dommett, G. H. B.; Kohlhaas, K. M.; Zimney, E. J.; Stach, E. A. et al. Graphene-Based Composite Materials. *Nature*, 2006, 442 (7100), 282–286.

[12] Novoselov, K. S.; Geim, A. K.; Morozov, S. V.; Jiang, D.; Zhang, Y.; Dubonos, S. V. et al. Electric Field Effect in Atomically Thin Carbon Films. *Science*, 2004, 306 (5696), 666–669.

[13] Kotov, N. A. Carbon Sheet Solutions. *Nature*, 2006, 442 (7100), 254–255.

[14] Avouris, P.; Chen, Z. H.; Perebeinos, V. Carbon-Based Electronics. *Nat. Nanotechnol.*, 2007, 2 (10) , 605–615.

[15] Navarro, C. G.; Burghard, M.; Kern, K. Elastic Properties of Chemically Derived Single Graphene Sheets. *Nano Lett.*, 2008, 8 (7), 2045–2049.

[16] Dikin, D. A.; Stankovich, S.; Zimney, E. J.; Piner, R. D.; Dommett, G. H.; Evmenenko, B. G. et al. Preparation and Characterization of Graphene Oxide Paper. *Nature*, 2007, 448 (7152), 457–460.

[17] Wilson, N. R.; Pandey, P. A.; Beanland, R.; Young, R. J.; Kinloch, I. A.; Gong, L. et al. Graphene Oxide: Structural Analysis and Application as a Highly Transparent Support for Electron Microscopy. *ACS Nano*, 2009, 3 (9), 2547–2556.

[18] Rourke, J. P.; Pandey, P. A.; Moore, J. J.; Bates, M.; Kinloch, I. A.; Young, R. J. et al. The Real Graphene Oxide Revealed: Stripping the Oxidative Debris from the Graphene-Like Sheets. *Angew. Chem., Int. Ed.*, 2011, 50 (14), 3173–3177.

[19] Morimune, S.; Nishino, T.; Goto, T. Ecological Approach to Graphene Oxide Reinforced Poly (methyl methacrylate) GO Nanocomposites. *ACS Appl. Mater. Interfaces,* 2012, 4 (7), 3596–3601.

[20] Morimune, S.; Nishino, T.; Goto, T. Poly(vinyl alcohol) Graphene Oxide Nanocomposites Prepared by a Simple Eco-Process. *Polym. J.*, 2012, 44 (10), 1056–1063.

[21] Xu, Y.; Hong, W.; Bai, H.; Li, C.; Shi, G. Strong and Ductile Poly (vinyl alcohol)/Graphene Oxide Composite Films with a Layered Structure. *Carbon,* 2009, 47 (15), 3538–3543.

[22] Liang, J.; Houng, Y.; Zhang, L.; Wang, Y.; Ma, Y.; Guo, T. et al. Molecular Level Dispersion of Graphene into Poly (vinyl alcohol) and Effective Reinforcement of their Nanocomposites. *Adv. Funct. Mater.*, 2009, 19 (14), 2297–2302.

[23] Kim, H. M.; Lee, J. K.; Lee, H. S. Transparent and High Gas Barrier Films Based on Poly(vinyl alcohol)/Graphene Oxide Composites. *Thin Solid Films,* 2011, 519 (22), 7766–7771.

[24] Zhao, X.; Zhang, Q.; Chen, D.; Lu, P. Enhanced. Mechanical Properties of Graphene-Based Poly(vinyl alcohol) Composites. *Macromolecules*, 2010, 43 (5), 2357–2363.

[25] Putz, K. W.; Compton, O. C.; Palmeri, M. J.; Nguyen, S. T.; Brinson L. C. High-Nanofiller-Content Graphene Oxide-Polymer Nanocomposites Via Vacuum-Assisted Self-assembly. *Adv. Funct. Mater.* 2010, 20 (19), 3322–3329.

[26] Podsiadlo, P.; Kaushik, A. K.; Arruda, E. M.; Waas, A. M.; Shim, B. S.; Xu, J. et al. Ultrastrong and Stiff Layered Polymer Nanocomposites. *Science*, 2007, 318 (5847), 80–83.

[27] Walther, A.; Bjurhager, I.; Malho, J. M.; Pere, J.; Ruokolainen, J.; Berglund, L. A. et al. Large-Area, Lightweight and Thick Biomimetic Composites with Superior Material Properties via Fast, Economic, and Green Pathways. *Nano Lett.*, 2010, 10 (8), 2742–2748.

[28] Shim, B. S.; Zhu, J.; Jan, E.; Critchley, K.; Ho, S.; Podsiadlo, P. et al. Multiparameter Structural Optimization of Single-Walled Carbon Nanotube Composites: Toward Record Strength, Stiffness, and Toughness. *ACS Nano*, 2009, 3 (7), 1711–1722.

[29] Stachewicz, U.; Modaresifar, F.; Bailey, R. J.; Peijs, T.; Barber, A. H. Manufacture of Void-Free Electrospun Polymer Nanofiber Composites with Optimized Mechanical Properties. *ACS Appl. Mater. Interfaces*, 2012, 4 (5), 2577−2582.

[30] Liu, A.; Walther, A.; Ikkala, O.; Belova, L.; Berglund, L. A. Clay Nanopaper with Tough Cellulse Nanofiber Matrix for Fire Retardancy and Gas Barrier Function. *Biomacromolecules*, 2011, 12 (3), 633–641.

[31] Hummers, W. S.; Offeman, R. E. Preparation of Graphitic Oxide. *J. Am. Chem. Soc.*, 1958, 80 (6), 1339–1339.

[32] Begam, T.; Nagpal, A.; Singhal, R. A. Comparative Study of Swelling Properties of Hydrogels Based on Poly (acrylamide-*co*-methyl methacrylate) Containing Physical and Chemical Crosslinks. *J. Appl. Polym. Sci.*, 2003, 89 (3), 779–786.

[33] Barati, A.; Norouzi, H.; Sharafoddinzadeh, S.; Davarnejad, R. Swelling Kinetics Modelling of Cationic Methacrylamide-Based Hydrogels. *World Appl. Sci. J.*, 2010, 11 (11), 1336–1341.

[34] Talyzin, A. V.; Sundqvist, B.; T. Szabo, T.; I. Dekany I.; Dmitriev, V. Pressure-Induced Insertion of Liquid Acetone into the Graphite. Oxide Structure. *J. Am. Chem. Soc.*, 2009, 131 (51), 18445–18449.

[35] Fan, Z.; Kai, W; Yan, J; Wei, T.; Zhi, L-J.; Feng, J. et al. Facile Synthesis of Graphene Nanosheets via Fe Reduction of Exfoliated Graphite Oxide. *ACS Nano*, 2011, 5 (1), 191–198.

[36] Yalcin, B.; Ergungor, Z.; Konishi, Y.; Cakmak, M.; Batur, C. Molecular Origins of Toughening Mechanism in Uniaxially Stretched Nylon 6 Films with Clay Nanoparticles, *Polymer*, 2008, 49 (6), 1635–1650.

[37] Zurayk, R. A.; Jones, E. H.; McNally, T.; Menary, G.; Martin, P.; Armstrong, C. Biaxial Deformation Behavior and Mechanical Properties of a Polypropylene/Clay Nanocomposite. *Compos. Sci. Technol.*, 2009, 69 (10), 1644–1652.

[38] Nakamura,Y.; Okabe, S.; Iida, T. Effects of Particle Shape, Size and Interfacial . Adhesion on The Fracture Strength of Silica-Filled Epoxy Resin. *Polym. Polym. Compos.*, 1999, 7 (10), 177–186.

[39] Wang, K.; Chen, L.; Wu, J.; Toh, M. L.; He, C.; Yee, A. F. Epoxy Nanocomposites with Highly Exfoliated Clay: Mechanical Properties and Fracture Mechanisms. *Macromolecules*, 2005, 38 (3), 788–800.

[40] Zhang, X.; Liu, T.; Sreekumar, T. V.; Hu, X.; Smith, K. Gel Spinning of PVA/SWNT Composite fibre. *Polymer*, 2004, 45 (26), 8801–8807.

[41] Pietralla, M.; Weeger, R. M.; Mergenthaler, D. B. The Role of Phonon Focusing and Structure Scattering in Oriented Semicrystalline Polymers. Z. *Eur. Phys. J. B.*, 1989, 77 (2), 219–228.

[42] Mergenthaler, D. B.; Pietralla, M.; Roy, S.; Kilian. H. G. Thermal Conductivity in Ultraoriented Polyethylene. *Macromolecules*, 1992, 25 (13), 3500–3502.

[43] Abdrashitov, E.; Bokun, V.; Kritskaya, D.; Ponomarev, A. Investigation of Poly(vinylidene chloride) Distribution in Perfluorinated Cation-Exchange Membranes MF-4SK upon UV- and γ-Initiated Graft Polymerization *High Energy Chem.*, 2008, 42 (6), 419–425.